Loss Mechanisms Determining the Quality Factors in Quartz Tuning Forks Vibrating at the Fundamental and First Overtone Mode

Pietro Patimisco, Angelo Sampaolo, Verena Mackowiak, Hubert Rossmadl, Alex Cable, Frank K. Tittel and Vincenzo Spagnolo

***Abstract*— Quartz tuning forks (QTFs) are piezo-transducers that have been implemented for numerous applications, such as chemical gas sensing, atomic-force microscopy, rheology and industrial process control. The most important parameter for QTFs sensing application is the resonance quality factor. An experimental investigation and theoretical analysis of the influence of QTFs geometries on the quality factor *Q* of the flexural fundamental and first overtone resonance modes is reported. The resonance frequencies and related *Q*-factors for five different QTFs have been measured. The QTF response was recorded at different air pressures to investigate the influence of the surrounding medium on the *Q*-factor. A data analysis demonstrated that air viscous damping is the dominant energy dissipation mechanism for both flexural modes. Thermoelastic and support losses are additional contributions that depend on the QTF geometry. A study of the QTF damping mechanism dependence upon the prong geometry is also provided.**

***Index Terms*— Quartz tuning fork, Quality factor, Fundamental and overtone modes, Loss mechanisms.**

I. Introduction

THE quartz tuning fork (QTF) is one of the best acoustic resonators and has the form of a two-pronged fork. It represents the central component for timing and frequency applications, due to its high resonance frequency stability and precision [1]. However, in the last few years QTFs have been implemented also for several other applications, like atomic force microscopy (AFM) [2]-[4], near-field optical microscopy [5]; quartz-enhanced photoacoustic spectroscopy (QEPAS) for gas sensing applications [6]-[7], rheology [8] and gas pressure, density and viscosity measurements [9]. When the QTF is excited at one of its flexural resonance mode or their harmonics, the two prongs oscillate in counterphase. The center of mass remains at rest and all forces are compensated in the support connecting the two prongs. This is in contrast with a single resonating single cantilever beam, which has an oscillating center of mass that dissipates energy. The inverse piezoelectric effect allows to use an electrical excitation to both induce and detect an oscillation in a QTF. Timing applications required a QTFs' geometry and crystal cut optimized to provide a constant resonance frequency of 2^{15} (~32.7 kHz) over a wide temperature range [1]. For different applications, such as gas sensing, atomic force microscopy as well as a viscometer, accelerometer or gyroscope other QTFs parameters are fundamental. For example, having a stiffness as small as possible is crucial for atomic force microscopy applications [10], while for QEPAS gas sensing, the QTF resonance quality-factor *Q*, defined as the ratio of the total input energy into the device to the energy dissipated within a vibration cycle, is the most important parameter [11]. The QEPAS sensor signal can be expressed as $S \propto (Q \cdot P \cdot \alpha)$, where Q is the QTF resonance quality factor, α is the gas target absorption coefficient and P is the laser power. Furthermore, a high quality-factor also implies a small resonance bandwidth, which makes the resonator response more selective in detecting external excitations and high *Q*-values correspond to low dissipation losses. To realize custom QTF resonators with a high *Q*-factor, it is important to understand the main physical factors contributing to the energy dissipation. The main energy dissipation mechanism occurring in a vibrating prong of a QTF are: damping by the surrounding fluid [12]-[14], support loss due to the interaction of the prong with its support [15]-[16], and thermoelastic damping [19]. All these loss mechanisms strongly depend on prong size and the dynamics of the vibrational mode under consideration. Several theoretical models have been proposed for each loss mechanism and their dependence on the main physical parameters have been reported. Each loss contribution is independent from the other, but all occur simultaneously for a vibrating QTF prong. To study how different loss mechanisms, contribute to the complete vibrational mode resonance *Q*-factor, we realized and studied a set of QTFs with different prong lengths, thicknesses and widths in an air pressure range from 20 torr to 760 torr. This investigation was performed for both the fundamental and first overtone in-plane flexural mode. Our analysis allows the separation of the contribution of the main loss mechanism due

Submission date: January 24th 2018.

The authors from Dipartimento Interateneo di Fisica di Bari acknowledge financial support from THORLABS GmbH, within PolySense, a joint-research laboratory. Frank K. Tittel acknowledges support by the Welch Foundation (Grant R492U).

P. Patimisco, A, Sampaolo, and V. Spagnolo are with PolySense Lab - Dipartimento Interateneo di Fisica, University and Politecnico of Bari, Via Amendola 173, Bari, Italy (e-mail: vincenzoluigi.spagnolo@poliba.it).

V. Mackowiak and H. Rossmadl are with Thorlabs GmbH, Hans-Boeckler-Straße 6, 85221 Dachau, Germany.

A. Cable is with Thorlabs, Inc., 56 Sparta Ave., Newton, 07860, USA

F. K. Tittel is with Department of Electrical and Computer Engineering, Rice University, 6100 Main Street, Houston, TX 77005, USA.

This article has been accepted for publication in a future issue of this journal, but has not been fully edited. Content may change prior to final publication. Citation information: DOI 10.1109/TUFFC.2018.2853404, IEEE Transactions on Ultrasonics, Ferroelectrics, and Frequency Control

to air damping, and an analysis of the dependence of the other two dissipation contributions on the prong geometry, i.e., support and thermoelastic losses.

II. Damping Mechanisms of a Cantilever Beam

A QTF can be treated as two identical cantilevers (prongs) coupled by a low-loss quartz bridge. Each prong can be approximated by a 2D-bar, since the crystal width is typically much smaller than the prong thickness and length. The Euler-Bernoulli beam theory describes the relationship between the deflection of the beam and its applied load and allows extraction of the discrete infinite natural resonance frequencies f_n for in-plane flexural modes given by [12]:

$$f_n = \frac{\pi T}{8\sqrt{12}L^2}\sqrt{\frac{E}{\rho}}m_n^2 \quad (1)$$

where E = $0.72\cdot10^{11}$ N/m^2 is the component of the quartz Young's modulus in the vibrating plane of the QTF and ρ = 2650 Kg/m^3 denotes the quartz density, T is the prong thickness, L its length and m_n is the mode number. The lowest resonance mode is usually referred to as the fundamental mode (m_0 = 1.194), while subsequent ones are called overtone modes (m_1 = 2.998 for the first overtone mode). High quality factors for a vibrational resonance mode result in low dissipation losses for the vibrating prongs and consequently a sharp frequency response. The main loss mechanisms in a QTF are due to: (i) air damping, related to the transfer of energy and momentum from the QTF prongs to the surrounding medium; (ii) support loss, related to transfer of mechanical energy from the vibrating prong to the support; (iii) thermoelastic damping, related to coupling between the strain field and the temperature field inside the QTF. Each resonance mode is characterized by a different vibration profile along the prongs axis with antinode points that identify the position of maximum vibration amplitudes along the prong. In other words, each vibrational mode is expected to exhibit a different quality factor because loss mechanisms are also dependent on the related vibrational dynamics [20]-[23].

When a QTF vibrating prong is immersed in air, a drag force is exerted on it. In the viscous region, the medium acts as a viscous fluid and the drag force is calculated using fluid mechanics. With the assumption that the length L of the QTF prong is much greater than its thickness T and crystal width w, Hosaka et al. [12] derived a formulation of the quality factor related to fluid damping (Q_{air}):

$$Q_{air} = \frac{4\pi\rho T w^2 f_n}{3\pi\mu w + \frac{3}{4}\pi w^2\sqrt{4\pi\rho_{air}\mu f_n}} \quad (3)$$

where ρ_{air} is the air density and μ its viscosity. In Fig. 1a, Q_{air} is plotted as a function of the pressure considering a QTF having L = 17 mm, T = 1.0 mm and w = 0.25 mm, for both the fundamental and the first overtone mode (μ =$1.81\cdot10^{-5}$ kg/m·s). $\rho_{air} = MP/R\Theta$ is estimated by using the ideal gas law, where M = 28.964 Kg/mol is the molar mass, R = 62.3637 m^3·Torr/K·mol is the gas constant and Θ (in K) is the prong temperature. In both cases, Q_{air} decreases very rapidly when the pressure increases from 25 torr to 150 torr. At higher pressures, Q_{air} levels off and becomes quasi-asymptotic at atmospheric pressure. The air damping mechanisms are strongly reduced for higher order vibrational modes. By combining Eq. (1) and Eq. (3), an explicit dependence of Q_{air} can be derived as a function of the prong size. In Fig. 1b, Q_{air} is plotted as a function on the ratio T/L, in which L ranges from 3 mm to 17 mm and 0.2 < T < 1.4 mm, for w = 0.25 mm and w = 0.5 mm. The data was simulated at an air pressure of 50 torr. For a fixed pressure and crystal width, a quasi-linear dependence of Q_{air} on the ratio T/L is observed. The guideline that emerges from this model is that to reduce viscous losses, the T/L ratio must be kept high. In addition, the lower the crystal thickness, the higher will be the air damping losses.

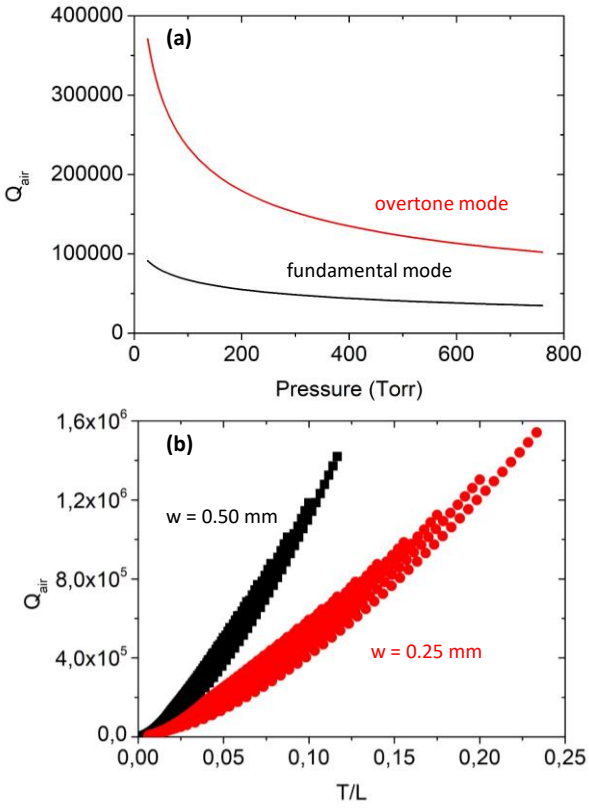

Fig. 1. (a) Q_{air} plotted as a function of the gas pressure for a QTF with a prong length and width of 17.0 mm and 1.0 mm, respectively and a crystal thickness of 0.25 mm for the fundamental (solid black curve) and the first overtone (solid red curve) mode. (b) Q_{air} plotted as a function of the ratio between the prong thickness T and its length L for a crystal thickness of w = 0.25 mm (●) and w= 0.5 mm (■) at an air pressure of 50 torr.

The simplest model to study support losses was developed by Hao et al. [17], in which the prong is supposed to be a rectangular cross-section resonator, attached monolithically to a larger support with the same thickness as that of the prong. The crystal thickness w is assumed to be much smaller than the elastic wavelength λ of the propagating waves. The closed-form expression for the quality factor related to the support loss in a clamped-free cantilever was expressed as:

$$Q_{supp} = A_n\frac{L^3}{T^3} \quad (4)$$

This article has been accepted for publication in a future issue of this journal, but has not been fully edited. Content may change prior to final publication. Citation information: DOI 10.1109/TUFFC.2018.2853404, IEEE Transactions on Ultrasonics, Ferroelectrics, and Frequency Control

with A_n coefficients depending on the resonance mode number and the prong material. Hao et al. estimated $A_0 = 2.081$ for the fundamental mode and $A_1 = 0.173$ for the first overtone mode.
Thermo-elastic dissipation is an intrinsic structural dissipation mechanism of the oscillating elements, which can be expressed using a modelling approach proposed by Zener [19]. The quality factor Q_{TED} related to thermo-elastic loss for an isotropic homogeneous beam can be expressed as:

$$Q_{TED} = \frac{\rho c_T}{E\beta^2\Theta} \cdot \frac{1+\left(\frac{2c_T f_n \rho T^2}{\pi\lambda_T}\right)^2}{\frac{2c_T f_n \rho T^2}{\pi\lambda_T}} \approx \frac{2(\rho c_T)^2 f_n T^2}{E\beta^2\Theta\pi\lambda_T} \propto \frac{T^3}{L^2} \quad (5)$$

where λ_T, c_T and β are the thermal conductivity, the heat capacity per unit mass and the thermal expansion of the prong. This expression is based on the assumption of an isotropic beam. By combining Eq. (1) and Eq. (5), in a first approximation, Q_{TED} scales with prong size as T^3/L^2.

III. Experimental Measurements

To investigate the dependence of loss mechanisms on the prong size of QTFs vibrating at the fundamental and overtone modes, a set of five different QTFs was designed and then realized. The geometrical properties of the QTFs are listed in Table I.
The QTFs were realized starting from a z-cut quartz wafer with a 2° rotation along the x-axis, since this crystal cut provides stable flexural vibrational modes frequencies at room temperature. Furthermore, the z-cut is the crystal-cut typically used for QTFs operating at low frequencies (up to 50 kHz). The quartz wafers were etched. A three-dimensional crystal structure is generated by chemical etching in a saturated aqueous solution of ammonium bifluoride. The temperature of the chemical etching solution was monitored directly by a temperature controller and kept at a constant 52 °C. This temperature was chosen because it allows chemical etching in a reasonable amount of time while also permitting adequate control of frequency by adjusting the etching time. Constant agitation was provided by a motor-driven rotary propeller. Electrodes, consisting of chromium (50 Å thick) and gold (250 Å thick) patterns, are applied photolithographically by means of shadow masks defined on both sides of the wafer. The gap between centre and side electrodes is 50 µm. A schematic of the investigated QTF set is shown in Fig. 2.

TABLE I
Dimensions of the custom tuning forks: *L* (prong length), *T* (prong thickness) and *w* (quartz crystal thickness).

QTF	Prong length L (mm)	Crystal width w (mm)	Prong thickness T (mm)
#1	3.5	0.25	0.2
#2	10.0	0.25	0.9
#3	10.0	0.50	1.0
#4	11.0	0.25	0.5
#5	17.0	0.25	1.0

The electrode layout was designed to enhance the fundamental flexural mode but allowing also the excitation of the first overtone mode. Due to the piezoelectricity of quartz, when a stress is applied to a QTF prong, a displacement of charge and a net electric field is induced. The effect is reversible and when a voltage is applied to a piezoelectric material, it is accompanied by a strain. Hence, the QTF response can be obtained by exciting the resonator electrically. The experimental setup used to characterize custom QTFs via electrical excitation is schematically depicted in Fig. 3. A waveform generator, Tektronix AFG 3102, generates a sinusoidal voltage excitation, which results in a piezoelectric charge distribution across the QTF prongs.

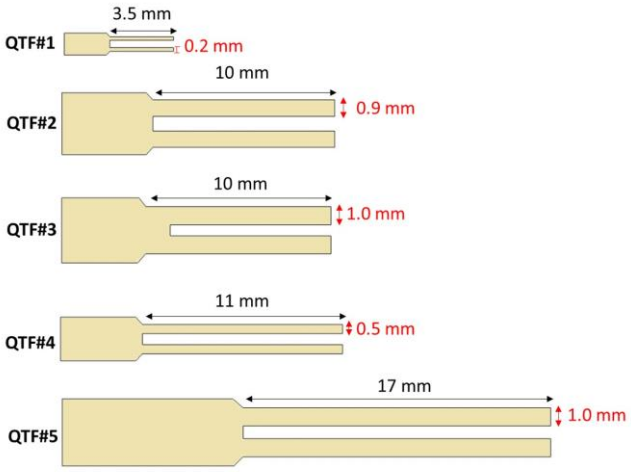

Fig. 2. Schematic of the investigated QTFs labelled as in Table I.

This piezoelectric current is then converted to an output voltage by means of a custom-made trans-impedance amplifier (TA) amplifier with a feedback resistor of 10 MΩ and gain factor of ~30. The TA output voltage is fed to a commercial lock-in amplifier (7265 Dual Phase DSP Lock-in Amplifier from Signal Recovery), which demodulates the signal at the same frequency of the waveform generator. The demodulated signal is then sent to a DAQ card (NI USB 6009), which is interfaced with a PC for data analysis. The QTF was mounted in a vacuum chamber. The vacuum chamber was connected with a gas line that included a pressure controller and an oil-free pump. In this way, it was possible to select and fix the air pressure in the vacuum chamber in the range between 20-760 torr.

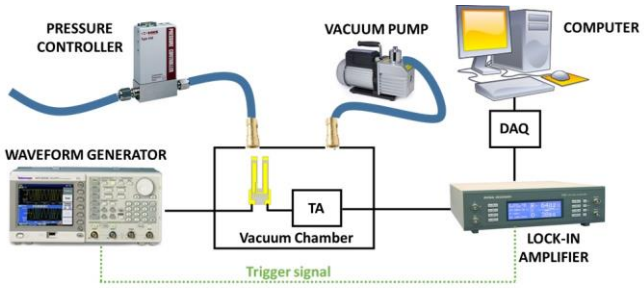

Fig. 3. Schematic of the experimental setup. TA – Trans-impedance amplifier; DAQ – Data acquisition card.

This article has been accepted for publication in a future issue of this journal, but has not been fully edited. Content may change prior to final publication. Citation information: DOI 10.1109/TUFFC.2018.2853404, IEEE Transactions on Ultrasonics, Ferroelectrics, and Frequency Control

IV. Measurements of Resonance Frequencies and Quality Factors

The Euler-Bernoulli equation can be used to predict the theoretical frequencies for the fundamental and the overtone modes. The actual values can be determined by performing a wide frequency range, using a custom-made LabVIEW-based software to vary step-by-step the frequency of the waveform generator (with an excitation peak-to-peak voltage of 0.5 mV) and acquire the lock-in output via the DAQ. As an example, Fig. 4 shows the spectral response of the QTFs at 50 torr. Once

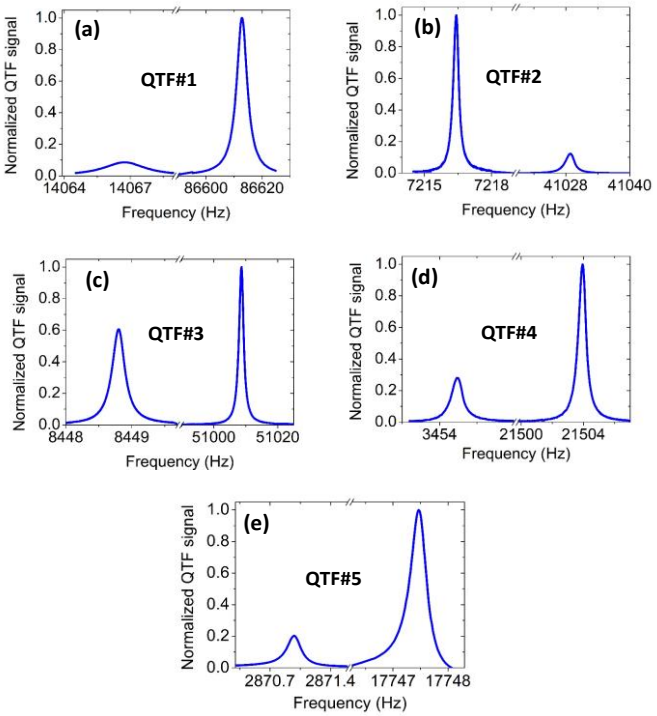

Fig. 4. QTFs resonance curves measured at a pressure of 50 Torr in standard air for QTF#1 (a), QTF#2 (b), QTF#3 (c), QTF#4 (d) and QTF#5 (e), for the fundamental and first overtone modes. In each graph, curves are normalized to the related highest signal value.

identified the center value, a well resolved resonance curve is obtained by applying a short frequency ramp (few mHz) around the peak. For each QTF, the fundamental and the overtone modes exhibit different peak values. The peak value is inversely proportional to the electrical resistance of the QTF, which is in turn inversely proportional to the Q factor. The QTFs electrical resistance values depend upon the prongs' geometry and resonance mode order [24]. Each spectral response was fitted by using a Lorentzian function to determine the resonance frequency, i.e., the peak value of the Lorentzian fit function and the full-width-half-maximum (FWHM) [25]. In Table II the extracted values for the resonance frequencies f_0 (fundamental mode) and f_1 (first overtone mode) at 50 torr are reported.

TABLE II
Resonance Frequencies of the Fundamental Mode (F_0) and the First Overtone Mode (F_1) Measured at 50 Torr of Air Pressure

QTF	f_0 (Hz)	f_1 (Hz)
#1	14068.14	86612.38
#2	7216.41	41028.76
#3	8448.80	51008.62
#4	3454.27	21503.81
#5	2870.98	17747.47

The FWHM was used to determine the quality factor as $Q = f/FWHM$ for the fundamental and overtone mode. Figure 5 depicts the extracted quality factor values for the investigated set of QTFs plotted as a function of the air pressure for both fundamental and first overtone modes.

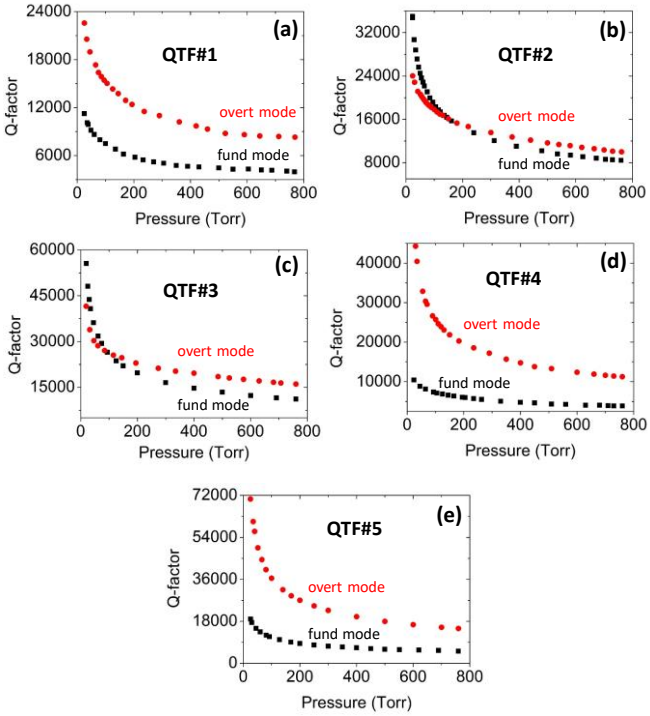

Fig. 5. Quality factors measured as a function of the air pressure for the flexural fundamental (■) and overtone (●) vibrational resonance modes, for QTF#1 (a), QTF#2 (b), QTF#3 (c), QTF#4 (d) and QTF#5 (e).

.

Apart from main loss mechanisms described in the previous paragraph, any asymmetry between prongs geometry results in an additional damping mechanism for the vibrating prong. The influence of prongs' asymmetries on the overall QTF quality factor has been reported in several publications using classical mechanical models [26]-[27]. For a standard 32.7 kHz-QTF (L = 3.5 mm, T = 0.3 mm and w = 0.3 mm), a prong symmetry breaking caused by a mass difference within 0.3% produces a decrease of the Q-factor of less than 10% [27]. For QTFs investigated in this work, such a fractional mass difference corresponds to a prong size variation of few microns for the shortest dimension (T for the investigated QTFs), assuming that the crystal width is not affected by the QTFs fabrication process. To experimentally evaluate the influence of the prongs size asymmetry on the overall quality factor, we performed a statistical study by testing different QTF samples having the same geometry and belonging to different crystal benches, with the same experimental conditions. All the QTF samples showed Q-factor values differing by less than 10%. This confirms that the QTFs fabrication process does not produce asymmetries in the prongs geometry that can affect the QTF Q-factor.

The dependence of the measured quality factors on air pressure follows the trend of Q_{air} reported in Fig. 1a, suggesting that the dominant loss mechanism is air damping for both

This article has been accepted for publication in a future issue of this journal, but has not been fully edited. Content may change prior to final publication. Citation information: DOI 10.1109/TUFFC.2018.2853404, IEEE Transactions on Ultrasonics, Ferroelectrics, and Frequency Control

modes. The air damping dependence on the prong size can also be investigated by comparing QTFs differing only in *T* or *L*.

QTF#2 and QTF#4 share almost the same prong length (*L* = 10 mm and *L* = 11 mm for QTF#2 and QTF#4, respectively) and the crystal thickness (*w* = 0.25 mm) but substantially differ in the prong thickness (T = 0.9 mm and T = 0.5 mm for QTF#2 and QTF#4, respectively). According to Fig. 1b, a reduction of the prong width corresponds to an increase of the air damping mechanisms. Indeed, at atmospheric pressure, the fundamental mode of QTF#2 exhibits a quality factor (*Q* = 8420), 2.2 higher than that measured for the QTF#4 (*Q*= 3870). Similarly, a reduction of the prong length causes an increase of the air damping mechanisms, when other prong sizes are equal. This statement has been verified by comparing QTF#2 (*L* = 10 mm, *w* = 0.25 and *T* = 0.9 mm) and QTF#5 (*L* = 17 mm, *w* = 0.25 and *T* = 1.0 mm), having almost the same *w* and *T* but differing in *L*. At atmospheric pressure the fundamental mode *Q*-factor of QTF#5 is 5210 is almost 1.6 times lower than that measured for the QTF#2. For the overtone modes, the air damping mechanisms are reduced (see Fig. 1a) and support losses start to dominate. Support losses strongly depend on the prong geometrical factor *L/T* (see Eq. (4)). In the investigated set of QTFs, the highest *L/T* ratios are 22, 17.5 and 17 calculated for QTF#4, QTF#1 and QTF#5, respectively. At atmospheric pressure, for these QTFs the *Q*-factor for the first overtone modes result in about three times higher with respect to the *Q*-factor measured for the fundamental modes. Conversely, for QTF#2 and QTF#3, only a slight increase of *Q*-factor is observed (*L/T* = 11.1 and 10.0 for QTF#2 and QTF#3, respectively). Since the dissipation mechanisms are assumed independent of each other and the resonator quality factor is proportional to the inverse of total energy dissipated, the overall *Q*-factor can be represented as a reciprocal sum of independent dissipative contributions:

$$\frac{1}{Q(P)} = \frac{1}{Q_{air(P)}} + \frac{1}{Q_{sup}} + \frac{1}{Q_{TED}} \quad (6)$$

Thermoelastic and support losses are assumed to be independent to the air pressure [17]-[19], and therefore it is possible to define *Q(0)* as:

$$\frac{1}{Q(0)} = \frac{1}{Q_{sup}} + \frac{1}{Q_{TED}} \quad (7)$$

where Q_{air} in Eq. (3) can be expressed as a function of gas pressure by using the general gas law:

$$Q_{air}(P) = \frac{a}{b+c\sqrt{P}} \quad (8)$$

where $a = 4\pi\rho T w f_n$, $b = 3\pi\mu$ and $c = 0.75\cdot\pi\mu w\,(4\pi M f_n \mu / N_A k_B \Theta)^{1/2}$, since $\rho_{air} = MP/N_A k_B \Theta$, where *M* is the molar mass of air, N_A is Avogadro's number, and k_B is the Boltzmann constant. As defined, *Q(0)* does not include the pressure-independent contribution derived from Hosaka's model [12]. By combining Eq. (6), Eq. (7) and Eq. (8), the overall *Q*-factor can be rewritten as:

$$Q(P) = \frac{1}{A+B\sqrt{P}} \quad (9)$$

where $A = 1/Q(0) + b/a$ and $B = c/a$. This equation was used to fit the experimental data reported in Fig. 5, both for the fundamental and overtone mode. As representative, the experimental data and the best fit obtained by using Eq. (9) for QTF#5 are reported in Fig. 6 for the fundamental and first overtone modes.

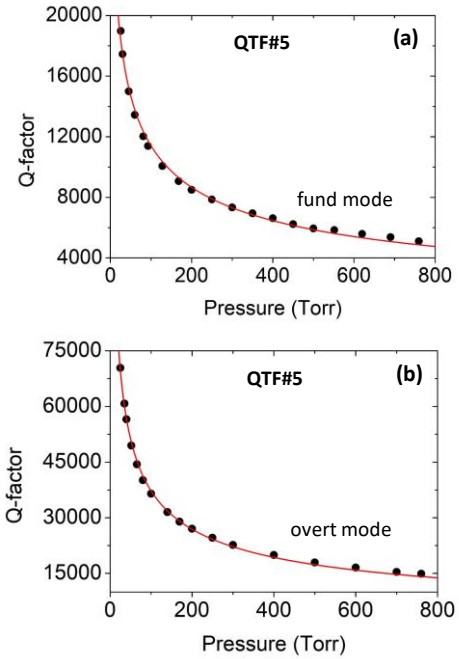

Fig. 6. Experimental quality factor values (●) as a function of the air pressure together with the best fit obtained by using Eq. (9) when QTF#5 oscillates at the fundamental (a) and the first overtone (b) mode.

.

The pressure-independent quality factor contribution *Q(0)* can be extracted by subtracting *b/a* from the fitting parameter *A*, leading to $1/Q(0) = A - b/a$. Hosaka's model [12] was used to calculate the ratio *b/a* in order to estimate *Q(0)*. In Table III, *A* and *B* values extracted from the fit together with *Q(0)* values for the fundamental and overtone mode are listed for all the investigated QTFs.

TABLE III
A AND B FITTING PARAMETERS OBTAINED BY USING EQ. (9), CALCULATED BY USING EQ. (3), EQ. (8) AND EQ. (9), AND *Q(0)* VALUES FOR THE FUNDAMENTAL AND THE FIRST OVERTONE MODES OF THE QTF SET INVESTIGATED IN THIS WORK.

	Fundamental mode			Overtone mode		
QTF	**A**	**B**	**Q(0)**	**A**	**B**	**Q(0)**
	$\cdot 10^{-6}$	**$\cdot 10^{-6}$ torr$^{-0.5}$**	**$\cdot 10^{3}$**	**$\cdot 10^{-6}$**	**$\cdot 10^{-6}$ torr$^{-0.5}$**	**$\cdot 10^{3}$**
#1	53.6	7.8	21.6	28.8	3.53	36.2
#2	8.9	4.35	174	31.1	2.49	32.6
#3	2.6	3.6	184	20	1.6	51.1
#4	62.6	7.37	19.7	6.7	3.15	209
#5	20.3	6.9	75.6	1.7	2.52	100

Each contribution to *Q(0)*, Q_{TED} and Q_{sup}, can be related with the geometrical properties of resonator: $Q_{sup} \propto L^3/T^3$, while $Q_{TED} \propto T^3/L^2$. With the analysis presented in this work, it is not possible to separate the two contributions of *Q(0)*. However it is feasible to investigate the dependence of *Q(0)* values from the geometrical parameters of the QTF prong, since Q_{sup} and Q_{TED} show opposite behaviors with the prong sizes.

This article has been accepted for publication in a future issue of this journal, but has not been fully edited. Content may change prior to final publication. Citation information: DOI 10.1109/TUFFC.2018.2853404, IEEE Transactions on Ultrasonics, Ferroelectrics, and Frequency Control

Figure 7a shows a clear linear dependence of *Q(0)* values on T^3/L^2 ratios, which proves that the relevant dissipation mechanism at the fundamental mode is related to the thermoelastic losses and support losses can be neglected.

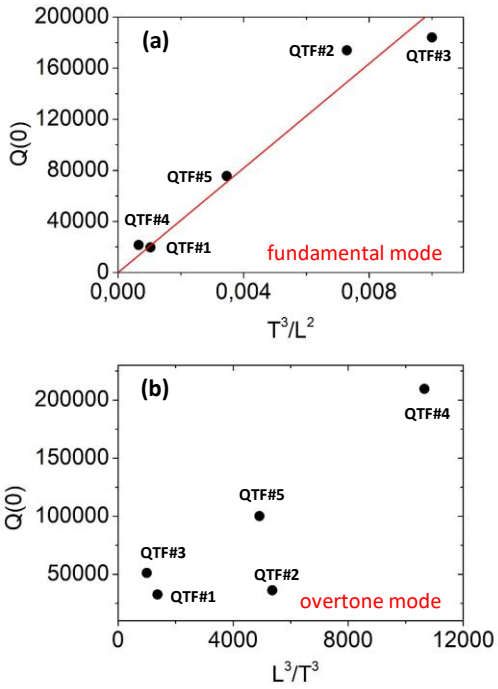

Fig. 7. *Q(0)* values (●) plotted as a function of the ratio T^3/L^2 for the fundamental mode (a) and as a function of L^3/T^3 for the first overtone mode (b). The red solid line is the best linear fit.

This agrees with the results obtained in Ref. [20] in which the support losses were negligible for QTFs vibrating at the fundamental mode, since an empirical correlation between the quality factor and *Tw/L* parameter at a pressure as low as 50 torr was observed (see. Fig. 1). Conversely, for the overtone mode, *Q(0)* values are positively correlated with L^3/T^3, as shown in Fig. 7b, indicating that the support losses contribution is not negligible for the overtone modes, even if a contribution due to thermoelastic damping is assumed to be present. This result agrees with the theoretical model proposed by Hao (see Eq. (4)) that predicts an increase of the support losses of a factor of A_0/A_1 ~ 12 when transitioning from the fundamental mode to the overtone mode.

V. Conclusions

In this work, the dependence of QTFs fundamental and first overtone flexural resonance modes *Q* factors on the dimensions of the prongs was investigated. This analysis was performed employing an experimental setup allowing the acquisition of the spectral response of an electrically excited tuning fork in the pressure range between 20-760 torr. A set of five tuning QTFs differing in prong sizes was realized and tested. All QTFs were excited both at the fundamental and the first overtone in-plane flexural mode resonance frequencies. The *Q* factor significantly decreases when the pressure increases from 20 Torr to atmospheric pressure. This behaviour suggested that a QTF mainly loses energy via the interaction with the surround viscous medium. The air damping mechanism was modelled by using an analytical expression derived by Hosaka et al. [13] and found to be in excellent agreement with the experimental data. Two other mechanisms of losses, pressure-independent and strongly dependent on the prong geometry, were considered: support and thermoelastic losses. The analysis proposed did not allow to separate these two contributions. However, the two mechanisms showed opposite trends with the prong geometry: the support loss contribution varies as L^3/T^3 while thermoelastic losses scale as T^3/L^2. By using such dependences, our results showed that support losses can be neglected at the fundamental mode while they became relevant for the overtone mode. In particular, air damping is reduced at the first overtone mode with respect to the fundamental mode and support losses become the relevant mechanism of energy dissipation at low pressures. All these results represent a guideline for the design of QTFs optimized for QEPAS applications. Typically, for QEPAS gas sensing the fundamental flexural resonance mode is exploited for optoacoustic detection. However, recently QEPAS sensors implementing QTF operating at the 1st overtone flexural mode have been demonstrated [20], [21], [28-29]. Therefore, by an appropriate design of the QTF prongs geometry it is possible to realize QTFs having high Q-factors selectively for the fundamental or the 1st overtone mode resonances.

Finally, it is worth noting that although the dependence of support losses on the prong geometry was verified, analytical models proposed in literature did not allow an exact calculation of the contributions to the overall *Q* factor due to support and thermoelastic losses. Hence, this study confirmed the limit of analytical models. Other computational methods (as for example, finite element method analysis) are mandatory for a precise prediction of the overall *Q* factor of a damped quartz tuning fork.

Acknowledgments

The authors from Dipartimento Interateneo di Fisica di Bari acknowledge financial support from THORLABS GmbH, within PolySense, a joint-research laboratory. Frank K. Tittel acknowledges support by the Welch Foundation (Grant R492U).

References

[1] J.M. Friedt, É. Carry, "Introduction to the quartz tuning fork," *Am. J. Phys.*, vol. 75, pp. 415-422, 2007.

[2] R.D. Grober, J. Acimovic, J. Schuck, D. Hessman, P.J. Kindlemann, J. Hespanha, A.S. Morse, K. Karrai, I. Tiemann, S. Manus, "Fundamental limits to force detection using quartz tuning forks," *Rev. Sc. Instr.*, vol. 71, pp. 2776-2780, 2000.

[3] F.J. Giessibl, "Atomic resolution on Si (111)-(7×7) by noncontact atomic force microscopy with a force sensor based on a quartz tuning fork," *Appl. Phys. Lett.*, vol. 76, pp. 1470-1472, 2000.

[4] H. Gottlich, R. W. Stark, J. D. Pedarnig, and W. M. Heckl, "Noncontact scanning force microscopy based on a modified tuning fork sensor," *Rev. Sci. Instrum.*, vol. 71, pp. 3104-3107, 2000.

[5] F.J. Giessibl, "High-speed force sensor for force microscopy and profilometry utilizing a quartz tuning fork," *Appl. Phys. Lett.*, vol. 73, pp. 3956-3958, 1998.

[6] A. A. Kosterev, F. K. Tittel, D. Serebryakov, A. Malinovsky, and A. Morozov, "Applications of quartz tuning forks in spectroscopic gas sensing," *Rev. Sci. Instrum.*, vol. 76, pp. 043105:1-043105:9, 2005.

[7] P. Patimisco, A. Sampaolo, L. Dong, F.K. Tittel, V. Spagnolo, "Recent advances in quartz enhanced photoacoustic sensing," *Appl. Phys. Rev.*, vol. 5, 011106:1-011106:19, 2018.

[8] M. Gonzalez, H.R. Seren, G. Ham, E. Buzi, G. Bernero, M. Deffenbaugh, "Viscosity and Density Measurements Using Mechanical Oscillators in Oil and Gas Applications," *IEEE T. Instrum. Meas.*, vol. P99, pp. 1-7, 2017.

[9] D. Garg, V.B. Efimov, M. Giltrow, P.V.E. McClintock, L. Skrbek, W.F. Vinen, "Behavior of quartz forks oscillating in isotopically pure 4He in the T → 0 limit," *Phys. Rev. B*, vol. 85, pp. 144518:1-144518:13, 2012.

[10] B. Walter, E. Mairiaux, M. Faucher, "Atomic force microscope based on vertical silicon probes," *Appl. Phys. Lett.*, vol. 100, pp. 243101:1-243101:4, 2017.

[11] M. Christen, "Air and gas damping of quartz tuning forks," Sensor. Actuator., vol. 4, pp. 555-564, 1983.

[12] H. Hosaka , K. Itao, S. Kuroda, "Damping characteristics of beam-shaped micro-oscillators," *Sensor. Actuat. A-Phys.*, vol. 49, pp. 87-95, 1995.

[13] K. Kokubun, H. Murakami, Y. Toda, M. Ono, "A bending and stretching mode crystal oscillator as a friction vacuum gauge," *Vacuum*, vol. 34, pp. 731-735, 1984.

[14] F.R. Blom, S. Bouwstra, M. Elwenspoek, J.H.J. Fluitman, "Dependence of the quality factor of micromachined silicon beam resonators on pressure and geometry," *J. Vac. Sci. Technol. B*, vol. 10, pp. 19-26,1992.

[15] Y. Jimbo, K. Itao, "Energy loss of a cantilever vibrator," *J. Horological Inst. Jpn.*, vol. 47, pp. 1-15, 1968.

[16] D.M. Photiadisa, J.A. Judge, "Attachment losses of high Q oscillators," *Appl. Phys. Lett.*, vol. 85, pp. 482-484, 2005.

[17] Z. Hao, A. Erbil, F. Ayazi, "An analytical model for support loss in micromachined beam resonators with in-plane flexural vibrations. *Sensor. Actuat. A-Phys.*, vol. 109, pp. 156-164, 2003.

[18] J.A. Judge, D.M. Photiadis, J.F. Vignola, B.H. Houston, J. Jarzynski, "Attachment loss of micromechanical and nanomechanical resonators in the limits of thick and thin support structures," *J. Appl. Phys.*, vol. 101, pp. 013521:1-013521:11, 2007.

[19] C. Zener, "Internal Friction in Solids II. General Theory of Thermoelastic Internal Friction," *Phys. Rev.*, vol. 53, pp. 90-99, 1938.

[20] A. Sampaolo, P. Patimisco, L. Dong, A. Geras, G. Scamarcio, T. Starecki, F.K. Tittel, V. Spagnolo, "Quartz-enhanced photoacoustic spectroscopy exploiting tuning fork overtone modes," *Appl. Phys. Lett.*, vol. 107, pp. 231102:1-231102:4, 2015.

[21] P. Patimisco, A. Sampaolo, H. Zheng, L. Dong, F.K. Tittel, V. Spagnolo, "Quartz enhanced photoacoustic spectrophones exploiting custom tuning forks: a review," *Adv. Phys. X*, vol. 2, pp. 169-187, 2016.

[22] K. Kokubun, M. Hirata, M. Ono, H. Murakami, Y. Toda, "Frequency dependence of a quartz oscillator on gas pressure," *J. Vac. Sci. Technol. A*, vol. 3, pp. 2184-2187, 1985.

[23] W.E. Newell, "Miniaturization of tuning forks," *Science*, vol. 161, pp.1320-1326, 1968.

[24] M. Hirata, K. Kokubun, M. Ono, K. Nakayama, "Size effect of a quartz oscillator on its characteristics as a friction vacuum gauge," *J. Vac. Sci. Technol.* A, vol. 3, pp. 1742-1745, 1985.

[25] D. I. Bradley, M. J. Fear, S. N. Fisher, A. M. Guénault, R. P. Haley, C. R. Lawson, G. R. Pickett, R. Schanen, V. Tsepelin, and L. A. Wheatland, "Stability of flow and the transition to turbulence around a quartz tuning fork in superfluid ^{4}He at very low temperatures," *Phys. Rev. B*, vol. **89**, pp. 214503:1-214503:9, 2014.

[26] A. Castellanos-Gomez, N. Agraït, G. Rubio-Bollinger, "Dynamics of quartz tuning fork force sensors used in scanning probe microscopy," *Nanotechnology*, vol. 20, pp. 215502:1-215502:8, 2009.

[27] J. Rychen, T. Ihn, P. Studerus, A. Herrmann, K. Ensslin, "A low-temperature dynamic mode scanning force microscope operating in high magnetic fields," *Rev. Sci. Instrum.*, vol. 70, pp. 2765-2768, 1999.

[28] H. Zheng, L. Dong, A. Sampaolo, P. Patimisco, W. Ma, L. Zhang, W. Yin, L. Xiao, V. Spagnolo, S. Jia, F.K. Tittel, "Overtone resonance enhanced single-tube on-beam quartz enhanced photoacoustic spectrophone," *Appl. Phys. Lett.*, vol. 109, pp. 111103:1-111103:5, 2016.

[29] H. Wu, X. Yin, L. Dong, K. Pei, A. Sampaolo, P. Patimisco, H. Zheng, W. Ma, L. Zhang, W. Yin, L. Xiao, V. Spagnolo, S. Jia, F.K. Tittel, "Simultaneous dual-gas QEPAS detection based on a fundamental and overtone combined vibration of quartz tuning fork," *Appl. Phys. Lett.*, vol. 110, pp. 121104:1-121104:4, 2017.